# Multipath adiabatic quantum state transfer

Bing Chen,* Wei Fan, Yan Xu, Yan-Dong Peng, and Hui-Yun Zhang
*School of Science, Shandong University of Science and Technology, Qingdao 266510, China*
(Received 26 February 2013; revised manuscript received 10 July 2013; published 20 August 2013)

We study coherent adiabatic quantum state transfer through a multipath data bus by means of controlling on-site energies, and analyze the effect of pathway number on transfer efficiency. We first introduce a simple spacial geometry and demonstrate that the multipath data bus which contributes to the quantum state transfer can reduce to a tight-binding chain with three quantum dots. Simulation results show that the electron can be transferred more efficiently by properly increasing the number of transfer paths under the same shape of controlling pulses. The optimal pathway number and the corresponding high-fidelity transfer time scale are determined by the numerical analysis. Finally, we extend our proposal to a more general system. The results show that such a scheme is relatively insensitive to imperfect fabrications. Our discussions illuminate the possibility of system engineering to enhance control and transfer times.

DOI: 10.1103/PhysRevA.88.022323 PACS number(s): 03.67.Hk, 03.65.−w, 73.23.Hk

## I. INTRODUCTION

Nowadays quantum state transfer (QST) based on adiabatic passage has attracted increasing attention. A variety of adiabatic schemes for high-fidelity transfer have been proposed. Compared to other mechanisms of QST, adiabatic passage for coherent QST has the following advantages. First, the adiabatic way of QST has the property of being robust against weak variations of the Hamiltonian. Hence, this method is more feasible in experiment. Second, as long as the change of the system parameters is adiabatic, the transfer timing does not need to be controlled precisely. Once the transfer has been accomplished, the system will be frozen to a steady state.

In a three-level quantum system, stimulated Raman adiabatic passage (STIRAP) [1] is a robust technique for coherent population transfer, in which the population is transferred adiabatically between two internal quantum states of an atom by maintaining the system in the dark state. Recently this adiabatic method has been extended to a variety of solid-state systems to realize coherent QST. The solid-state system makes it possible for scale-up of quantum computing devices. Among these, coherent tunneling via adiabatic passage (CTAP) [2] is a typical scheme for coherently spatial particle transfer in quantum dot (QD) systems. A similar scheme has been independently proposed for neutral atoms in optical traps [3]. In such a scheme, the particle is driven by slowly changing the tunneling interaction between the nearest neighboring quantum units, which has been demonstrated in an engineered optical waveguide system to control light propagation [4,5]. The CTAP technique has been proposed for creating a maximally coherent superposition in a two-state atom [6], and manipulating single atoms in optical lattice [7–9], electron spin states in two-dimensional architecture [10], and Bose-Einstein condensates [11,12]. It has also been applied to the problem of transferring quantum state across the chain for realizing long-range QST [13–15], quantum fan-out [16], and electron interferometry [17]. More realistic problems have also been discussed for the experimental observation of CTAP in QDs system [18,19].

Another way to realize high-fidelity QST can be achieved via adiabatic manipulation of the on-site energy applied on QDs. Reference [20] has shown a method for the creation of spatially separated spin entanglement. Based on the fact that the tunneling dynamics of the electron depends strongly on the on-site energy, Ref. [21] has presented a scheme to adiabatically transfer an electron from one end to the other end of a three-dot array using the ground state of the system. Different from the CTAP process, the protocol in Ref. [21] considered a system with *time-independent* interactions, instead, the on-site energies of the two external dots (sender and receiver) could be manipulated and the transfer dynamics was more stable by maintaining the system in the ground state. It was a high-fidelity process for a proper choice of system parameters and also robust against experimental parameter variations. Moreover, this protocol can be easily extended to the problem of long-range QST [22,23].

In this paper we present a detailed analysis of adiabatic QST through a multipathway data bus, which is schematically illustrated in Fig. 1(a). A similar scheme has been realized in an optical waveguide system [5]. In our scheme, the sender ($A$) and receiver ($B$) are controlled by the external gate voltages, respectively. Our aim is to move the particle from one end of the system to the other efficiently in the shortest possible time. We show that the overall dynamics of this scheme is equivalent to that in a five-dot tight-binding chain. We first investigate the effect of system parameters on the minimum energy gap between lowest two eigenstates and the transfer fidelity. We then show that the electron can be robustly transported from one end of the chain to the other, by slowly varying the gate voltages. Finally, the optimal parameter values and the time scale to realize high-efficiency transfer are determined. The scheme in this paper are not proposed as realistic experimental devices. Rather, the point is to illustrate through constructive, analytic, protocols how the desired solutions can arise efficiently for some class of schemes.

This paper is organized as follows: In Sec. II the QST protocol is setup and the property of the ground state is investigated via a Bethe ansatz method. In Sec. III the transport of the quantum state based on this scheme is discussed. Finally, we summarize the results in Sec. IV.

*chenbingphys@gmail.com

 

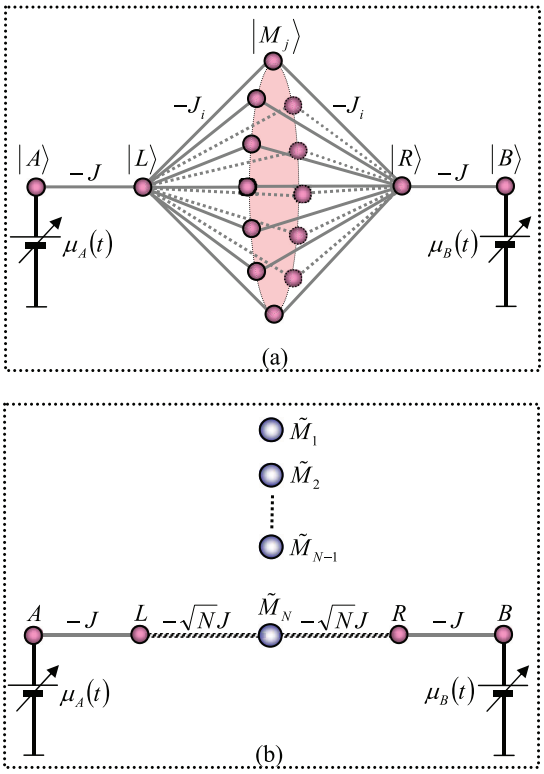


FIG. 1. (Color online) (a) Schematic illustration of a multipath data bus for adiabatic QST consisting of $N$ noninteraction QDs, each coupled with both the data bus ends QD-$L$, $R$. The sender $A$ and the receiver $B$ are coupled with two ends of the data bus, respectively. The system is controlled by gate voltages $\mu_\alpha(t)$ ($\alpha = A,\ B$). The coupling strength between all QDs is $-J$. By adiabatically varying the gate voltages, the particle is moved from QD-$A$ to QD-$B$. (b) The equivalent model of (a) after applying linear transformation. The whole system can reduce to $N-1$ noninteraction single sites and a five-site tight-binding chain. The coupling strengths between three inner sites are $-\sqrt{N}J$.

## II. MULTIPATH SYSTEM

The multipath transfer scheme is illustrated in Fig. 1(a). The whole quantum system consists of two QDs (the sender $A$ and the receiver $B$) which are controlled by external gate voltages and coupled with a $N$-path quantum data bus that is formed by two ends coupled with $N$-independent QDs. The total Hamiltonian reads

$$\mathcal{H}(t) = -J(a_A^\dagger a_L + a_B^\dagger a_R) - \sum_{j=1}^{N} J_j(a_L^\dagger + a_R^\dagger)a_{M_j} + \mu_A(t)a_A^\dagger a_A + \mu_B(t)a_B^\dagger a_B + \text{H.c.}, \tag{1}$$

where $J$ and $J_j$ are ferromagnetic coupling constants. For simplicity we assume that the coupling strengths between the nearest neighboring QDs are all equal and negative, $J_i = J$. And $a_j$ is the annihilation operator on site $j$ for $j = A, L, M_1, \ldots, M_N, R, B$; $\mu_A(t)$ and $\mu_B(t)$ are the on-site energy (externally controlled) applied on the QDs. We write

$$\mu_A(t) = -\mu_0 f(t), \tag{2a}$$

$$\mu_B(t) = -\mu_0 f(t - t_{\max}), \tag{2b}$$

where $t_{\max}$ ($t_{\max} \gg 1/J$) is the total evolution time; $\mu_0$ is peak amplitude of the pulses; $f(t)$ is the general pulse-shape function which satisfies

$$f(0) = 1, \tag{3}$$

and monotonically goes to zero at $t \to \pm\infty$,

$$\lim_{t\to\pm\infty} f(t) = 0. \tag{4}$$

In this scheme we will consider the single particle case and denote the state with the particle occupying site $j$ by $|j\rangle \equiv a_j^\dagger|0\rangle$. First we initialize the particle occupied in QD-$A$, and keep the other QDs all empty at $t = 0$. The aim of this scheme is to transport the particle from the left end to the right end by maintaining the system in its ground state.

To find an analytical expression of the ground state, we simplify the Hamiltonian (1) by introducing the Fourier transformation

$$\tilde{a}_{M_p} = \frac{1}{\sqrt{N}} \sum_{j=1}^{N} e^{ipj} a_{M_j}, \tag{5}$$

where $p = 2m\pi/N$, $m \in [1, N]$ denotes the momentum. Substituting Eq. (5) into Eq. (1), the Hamiltonian can be reduced to be

$$\mathcal{H}(t) = -J[a_A^\dagger a_L + \sqrt{N}(a_L^\dagger + a_R^\dagger)\tilde{a}_{M_N} + a_B^\dagger a_R + \text{H.c.}] + \mu_A(t)a_A^\dagger a_A + \mu_B(t)a_B^\dagger a_B. \tag{6}$$

Note that Eq. (6) is equivalent to $(N-1)$ noninteracting empty sites and a five-site tight-binding chain, which is schematically shown in Fig. 1(b). We see that the subsequent system evolution is confined to a Hilbert space spanned by the five vectors $\{|j\rangle | j = A, L, \tilde{M}_N, R, B\}$, which is only a subspace of the original $(N+4)$-dimensional Hilbert space. It is worth mentioning that a special case of this equivalence of actions was recently noted for the $XY$ Hamiltonian [24,25].

For a single-particle problem, we can write down all the eigenstates of Eq. (6) via the Bethe ansatz method which we write as $|\mathcal{D}_k(t)\rangle = f_A^k|A\rangle + \sum_{j=L,M,R} f_j^k|j\rangle + f_B^k|B\rangle$. Substituting the discrete superposition state in the eigenequation $\mathcal{H}(t)|\mathcal{D}_k(t)\rangle = \varepsilon_k|\mathcal{D}_k(t)\rangle$, we can get the relations among all the expansion parameters,

$$-Jf_L^k + \mu_A(t)f_A^k = \varepsilon f_A^k, \tag{7a}$$

$$-Jf_A^k - \sqrt{N}Jf_M^k = \varepsilon f_L^k, \tag{7b}$$

$$-\sqrt{N}J\left(f_L^k + f_R^k\right) = \varepsilon f_M^k, \tag{7c}$$

$$-\sqrt{N}Jf_M^k - Jf_B^k = \varepsilon f_R^k, \tag{7d}$$

$$-Jf_R^k + \mu_B(t)f_B^k = \varepsilon f_B^k. \tag{7e}$$

From the equations above, we can write down all the eigenstates of Hamiltonian (6). In this proposal we will use the ground state $|\mathcal{D}_g(t)\rangle$ of Hamiltonian $\mathcal{H}(t)$ to implement the population transfer from state $|A\rangle$ to state $|B\rangle$. By straightforward calculation, we get the normalized ground

state $|\mathcal{D}_g(t)\rangle$, which is

$$|\mathcal{D}_g(t)\rangle = \frac{1}{\sqrt{\Lambda}}\{\sqrt{N}[N\sinh 5\kappa_g + (N-1)\sinh 3\kappa_g + \xi_B(t)\sqrt{N}\sinh 4\kappa_g]|A\rangle + [N\sinh 4\kappa_g + (N-1)\sinh 2\kappa_g + \xi_B(t)\sqrt{N}\sinh 3\kappa_g]|L\rangle + [N\sinh 3\kappa_g + (N-1)\sinh\kappa_g + \xi_B(t)\sqrt{N}\sinh 2\kappa_g]|M\rangle + [N\sinh 2\kappa_g + \xi_B(t)\sqrt{N}\sinh\kappa_g]|R\rangle + \sqrt{N}\sinh\kappa_g|B\rangle\}, \quad (8)$$

with the eigenvalue $\varepsilon = -2\sqrt{N}J\sinh\kappa_g$. Here $\Lambda$ is the normalization coefficient and $\kappa_g$ is determined by the condition

$$N(\xi_A-\varepsilon)(\xi_B-\varepsilon)\sinh 4\kappa_g + J^2\sinh 2\kappa_g = \sqrt{N}J(\xi_B+\xi_A-2\varepsilon)\sinh 3\kappa_g, \quad (9)$$

with $\xi_l = \mu_l(t)/J$, $l = A, B$, respectively.

Starting from $t = 0$, we have $\mu_A(0) = -\mu_0$ and $\mu_B(0) \approx 0$. The initial instantaneous ground state $|\mathcal{D}_g(0)\rangle$ reads

$$|\mathcal{D}_g(0)\rangle = \frac{1}{\sqrt{\Lambda_0}}\{\sqrt{N}[N\sinh 5\kappa_0 + (N-1)\sinh 3\kappa_0]|A\rangle + [N\sinh 4\kappa_0 + (N-1)\sinh 2\kappa_0]|L\rangle + [N\sinh 3\kappa_0 + (N-1)\sinh\kappa_0]|M\rangle + N\sinh 2\kappa_0|R\rangle + \sqrt{N}\sinh\kappa_0|B\rangle\}. \quad (10)$$

In this scheme, the transfer efficiency depends on various factors, one of which is the probability of finding $|A\rangle$ in $|\mathcal{D}_g(0)\rangle$, i.e., $\rho_A = N[N\sinh 5k_0 + (N-1)\sinh 3k_0]^2/\Lambda_0$. Large $\rho_A$ is necessary to achieve high-fidelity transfer. The value of $\rho_A$ is determined by two parameters: the ratio $\mu_0/J$ and the number of pathways $N$. In Fig. 2 we show the difference $1-\rho_A$ as a function of $\mu_0/J$ and $N$. We can see that for a given number of pathway $N$, $1-\rho_A$ decreases as $\mu_0/J$ grows, but increases as $N$ increases. This is because strong coupling strength will increase the probability of a particle occupying three middle sites. By choosing a sufficiently large value of $\mu_0$, the ground state $|\mathcal{D}_g(0)\rangle$ can be approximately reduced to $|A\rangle$. If we choose the peak value $\mu_0/J = 20$, and assume the probability of $|A\rangle$ in $|\mathcal{D}_g(0)\rangle$ greater than 0.996, the biggest allowed value of pathway number is 50.

In the time limit $t = t_{\max}$, the parameter $\mu_A(t)$ goes to zero and $\mu_B(t)$ goes to $-\mu_0$. For a proper choice of parameters we can see that the ground state of Eq. (10) evolves to be $|\mathcal{D}_g(t_{\max})\rangle \approx |B\rangle$ with the same reasoning as the above paragraph. One can see that initializing the system in state $|\Psi(t=0)\rangle = |A\rangle$ and adiabatically changing $\mu_A(t)$ and $\mu_B(t)$, the population will smoothly change to be $|B\rangle$, i.e.,

$$|\Psi(t=0)\rangle = |A\rangle \to |\Psi(t=t_{\max})\rangle = |B\rangle. \quad (11)$$

## III. DYNAMICAL EVOLUTION

The above analysis shows that if the time-dependent change is introduced slowly enough, the population remains in the ground state $|\mathcal{D}_g\rangle$ and is adiabatically transferred from state $|A\rangle$ to state $|B\rangle$ completely at $t = t_{\max}$. It is worth mentioning that in the adiabatic limit, the process does not depend on the shape of the pulses. However, this will not be the case in practice in such a scheme. For a given tolerable transfer error, a proper choice of the pulse can greatly reduce the possible time for implementing the transfer of the state. The pulse separation is an important factor affecting the transfer efficiency. We are now ready to consider the case that controlling pulses are modulated in Gaussian shape [shown in Fig. 3(a)]

$$f(t) = \exp\left[-\tfrac{1}{2}\alpha^2 t^2\right], \quad (12)$$

where $\alpha$ is standard deviation of the control pulse. The advantage of such pulse is that the pulse separation is varied as a function of $\alpha$. To choose optimal parameters for QST, it would be useful to discuss the relationship between adiabaticity and system parameters.

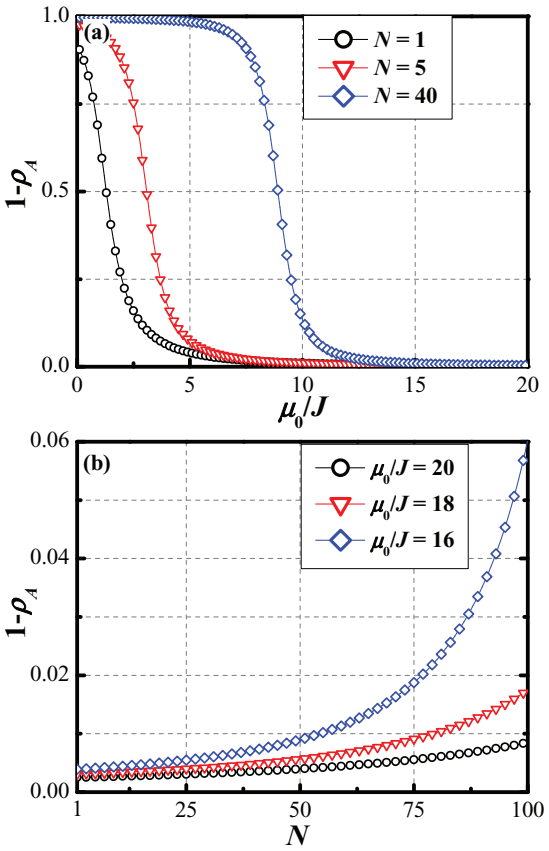


FIG. 2. (Color online) The probability of finding $|A\rangle$ in the instantaneous ground state $|\mathcal{D}_g(0)\rangle$ as a function of (a) the peak value $\mu_0/J$ for three different path numbers: $N = 1$ (circle), $N = 5$ (triangle), and $N = 40$ (diamond); and (b) the path number $N$ for three peak values: $\mu_0/J = 20$ (circle), $\mu_0/J = 18$ (triangle), and $\mu_0/J = 16$ (diamond). As the path number grows, larger peak values are needed to ensure large occupation probability of $|A\rangle$ in $|\mathcal{D}_g(0)\rangle$.

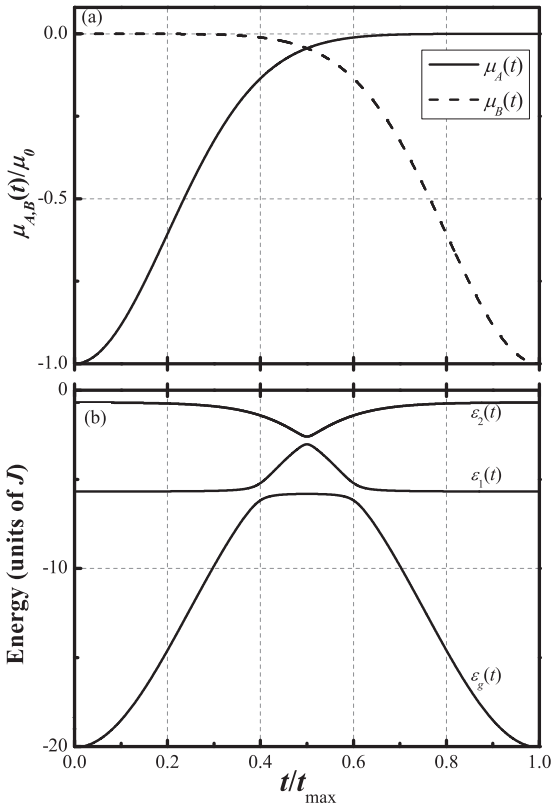


FIG. 3. (a) Gate voltages (in units of $\mu_0$) as a function of time (in units of $t_{max}$) described in Eq. (11). $\mu_A(t)$ is the solid line and $\mu_B(t)$ is the dashed line. (b) Energies of the lowest three eigenstates of 20-path quantum system as a function of time for the pulses shown in (a) with $\mu_0 = 20J$ and $\alpha = 4/t_{max}$. The eigenvalues exhibit avoided crossings during the evolution.

### A. Adiabaticity

In this section we will derive the condition to realize optimal transfer, which is measured by the adiabaticity parameter between the ground state and the first excited state

$$\mathcal{A}(t) = \left| \frac{\langle \dot{\mathcal{D}}_g(t) | \mathcal{D}_1(t) \rangle}{\varepsilon_g(t) - \varepsilon_1(t)} \right|. \tag{13}$$

For adiabatic evolution, the crucial requirement is $\mathcal{A}(t) \ll 1$ throughout the evolution, which suppresses the quantum transition from $|\mathcal{D}_g(t)\rangle$ to $|\mathcal{D}_1(t)\rangle$ during the transfer process. The necessary condition for this requirement is that the ground state and the first-excited state are nondegenerate during all the time evolution process. Taking the pathway number $N = 20$ as an example, to calculate instantaneous eigenvalues of the Hamiltonian (1) due to modulation of the gate voltages according to pulse equation (12) is generally only possible numerically. The energies of the lowest three eigenstates are calculated, which are plotted in Fig. 3(b). We observe there is no level crossing in our structure.

To illustrate the behavior more clearly, Fig. 4(a) presents the energy gap between two lowest eigenstates, i.e., $\delta(t) = \varepsilon_1(t) - \varepsilon_g(t)$, as a function of time for different pathways $N = 1, 2, 3, 4, 5, 10, 15$, and 20. Note that the gap approaches a nonzero minimum value, which plays a significant role in the transfer. This minimum energy gap plays an important role in our adiabatic scheme, which depends both on the pulse separations and number of pathways. In Fig. 4(b) the minimum gap is plotted as a function of the standard deviation $\alpha$ for three different values of pathways $N$. We can see that the minimum gap increases as $\alpha$ increases, and tends to a constant value which is related to the pathway number. The relation between the minimum gap and pathway number $N$ for $\alpha = 5/t_{max}$ is plotted in Fig. 4(c). It shows that the minimum gap can be improved by increasing the number of pathway $N$ and tends asymptotically towards a limiting value $J$. In a sense, increasing the number of path $N$ can increase the value of minimum gap in a limited range but not for the transfer efficiency completely. The reason is that, as mentioned above, the final instantaneous eigenstate is not the desired one for large $N$.

To determine the optimal pathway number $N$ for maximum transfer efficiency via our scheme, the adiabaticity of the evolution needs to be verified. As an example, we show in Fig. 5(a) $\mathcal{A}(t)\, t_{max}$ as a function of time for a system with $N = 20$ pathways. Comparing with Fig. 4(a), one can see that the adiabaticity is largest at the time of the energy gap reaching minimum. For a given finite transfer time $t_{max}$, it it necessary to discuss the effect of $N$ on adiabaticity. In Fig. 5(b), the maximal adiabaticity has now been determined in terms of $N$, which remains a free parameter, and therefore

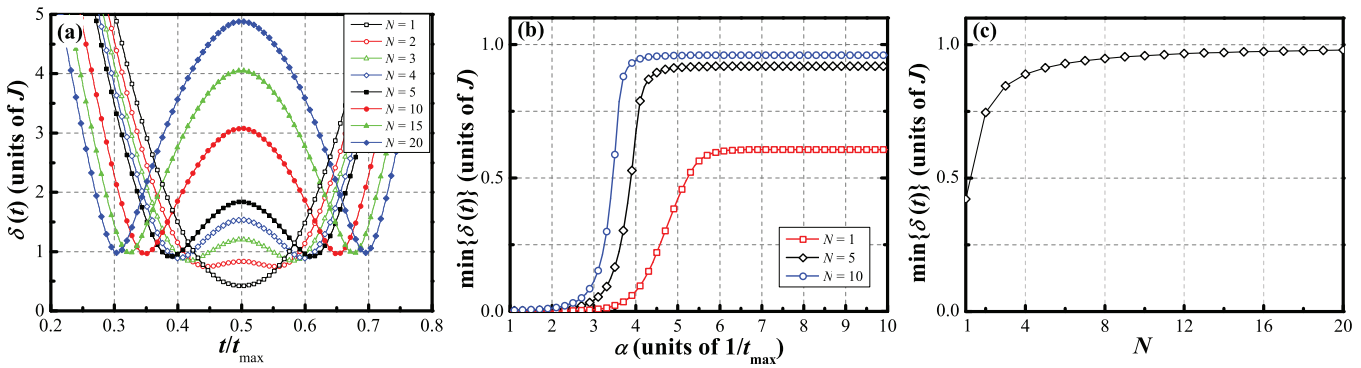


FIG. 4. (Color online) (a) The energy difference $\delta(t)$ between $\varepsilon_1(t)$ and $\varepsilon_g(t)$ as a function of time for different pathways $N = 1, 2, 3, 4, 5, 10, 15$, and 20. The parameters $\mu_0 = 20$ and $t_{max} = 150/J$, and the pulse deviation is $\alpha = 4/t_{max}$. The energy difference approaches an nonzero minimum gap during the evolution, which varies with pathway number. Effects of the (b) $\alpha$ and (c) path number on the minimum gap. It shows the gap can be increased by increasing $\alpha$ and $N$.

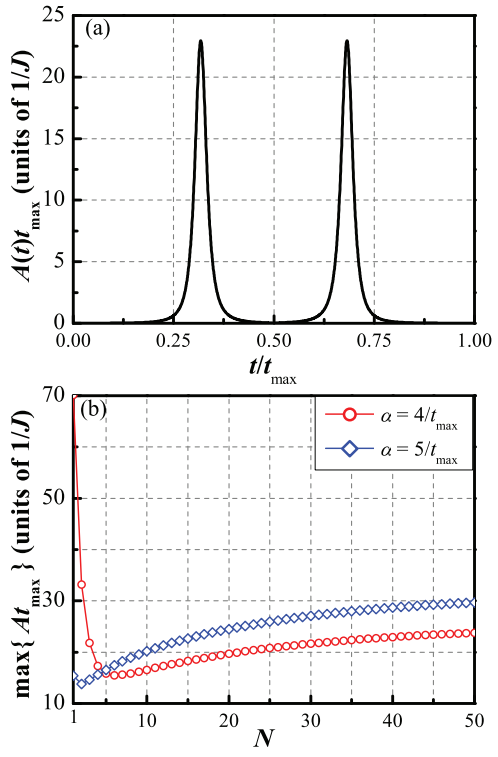


FIG. 5. (Color online) (a) Adiabaticity $\mathcal{A}(t)t_{\max}$ (in units of $1/J$) as a function of time. Parameters are the same as those in Fig. 4(a). The adiabaticity is largest at the time of the energy gap reaching minimum. (b) The maximal adiabaticity parameter max $\{\mathcal{A}(t)t_{\max}\}$ as a function of path number $N$ for $\alpha = 4/t_{\max}$ (circle), and $\alpha = 5/t_{\max}$ (diamond). We can see that there is an optimal choice of the pathway number that makes the transfer process most efficient by reducing the adiabaticity parameter and the transfer time to minimum. The optimal value of pathway number is $N = 5$ for $\alpha = 4/t_{\max}$, and $N = 2$ for $\alpha = 5/t_{\max}$.

allows for further optimization. For $\alpha = 4/t_{\max}$, the maximal adiabaticity decreases rapidly by increasing pathway number $N$ and reaches minimum value at $N = 5$. As we know, the smaller the adiabaticity, the shorter the time for high-fidelity transfer in a realistic experiment. In the present scheme, one can see that the optimal choice of path number is $N = 5$ for $\alpha = 4/t_{\max}$. On the other hand, the adiabaticity also depends on the parameter $\alpha$. The adiabaticity range is different for the different values of $\alpha$ as shown in Fig. 5(b). Obviously the optimal value of pathway number is $N = 2$ for $\alpha = 5/t_{\max}$. This suggests that the optimal value of pathway number varies with the pulse shape.

### B. The Schrödinger equation

Given an initial state $|\Psi(0)\rangle$, the consequent time evolution of the state is given by the Schrödinger equation

$$i\frac{d}{dt}|\Psi(t)\rangle = \mathcal{H}(t)|\Psi(t)\rangle . \tag{14}$$

The state $|\Psi(t)\rangle$ is expressed as a superposition of the five basis states

$$|\Psi(t)\rangle = c_A(t)|A\rangle + \sum_{j=L,M,R} c_j(t)|j\rangle + c_B(t)|B\rangle . \tag{15}$$

Equation (14) is solved with the initial conditions: $c_A(0) = 1$ and $c_m(0) = 0$, $m \neq A$. The probability of finding the target state $|B\rangle$ at time $t$ is given by $|c_B(t)|^2$ and the transfer fidelity of the transfer process is defined as

$$F = |\langle B|\ \Psi(t_{\max})\rangle|^2 = |c_B(t_{\max})|^2 . \tag{16}$$

To illustrate the process of QST, we numerically integrate Eq. (14) to highlight the dynamics. In order to show the effect of pathway number on the transfer efficiency, we choose $t_{\max} = 150/J$ and $\alpha = 4/t_{\max}, 5/t_{\max}$. The top row of Fig. 6 shows the time-dependent populations for $\alpha = 4/t_{\max}$ and two different values of pathways: $N = 1$ (a) and $N = 5$ (b), respectively. For $N = 1$, the transfer fidelity is approximately 3.6% and most population remains in the pathways (dotted, green curves). In contrast, the populations of the states $|A\rangle$ (dashed, black curves) and $|B\rangle$ (solid, red curves) are exchanged with a fidelity of 99.5% for $N = 5$. From Fig. 6(c) one can see that for a given transfer period $t_{\max}$, the adiabatic transfer can be achieved by increasing the pathway number $N$ and the scheme is successful in transferring about 99.5% of the population from QD-$A$ to QD-$B$. Too large $N$, however, as mentioned above, will eventually destroy the transfer efficiency. It is clear that $N = 5$ is an optimum pathway number for adiabatic transfer, which is the coincident with the conclusion of Fig. 5(b). Similarly, we plot the time-dependent populations for $\alpha = 5/t_{\max}$ in the bottom row of Fig. 6. The transfer fidelity is 99.5% for $N = 2$ [as shown in Fig. 5(d)] and 99% for $N = 5$ [as shown in Fig. 5(e)]. Figure 5(f) shows that the transfer dynamics becomes unstable as the pathway number increases for $\alpha = 5/t_{\max}$.

Figure 7 shows the transfer fidelity as a function of the total transfer time $t_{\max}$ for 1-, 2-, 3-, 4-, and 5-path systems by solving the Schrödinger equations with varying $t_{\max}$ for $\mu_0 = 20J$. The most economical choice of transfer time to achieve high-fidelity transfer is $t_{\max} = 150/J$ with the pathway number $N = 5$. Comparing with the case $N = 1$, we can see that by adding four additional paths the transfer time can be greatly reduced while still preserving the high-transfer fidelity, so adding a multipath data bus can improve the transfer efficiency greatly.

### C. Robustness to disorder

Next we will discuss the robustness of this scheme against fabrication disorder. Assume that the tunnel coupling of pathway in Hamiltonian (1) has a random but constant offset $\delta\epsilon_j$, i.e.,

$$J_j = J(1 - \delta\epsilon_j), \tag{17}$$

where $\delta$ is the maximum coupling offset bias, $\epsilon_j$ is drawn from the standard uniform distribution on the open interval $(0,1)$, and all $\epsilon_j$ are completely uncorrelated for all sites along the chain. In Fig. 8 we show the fidelity as a function of $N$, with $\mu = 20J$, $t_{\max} = 150/J$, $\alpha = 5/t_{\max}$, and $\delta = 0.1J$ and $0.2J$. Comparing with ideal, i.e., $\delta = 0$, we can see that weak fluctuation in the coupling strengths has little effect on the performance around the optimal data bus configuration.

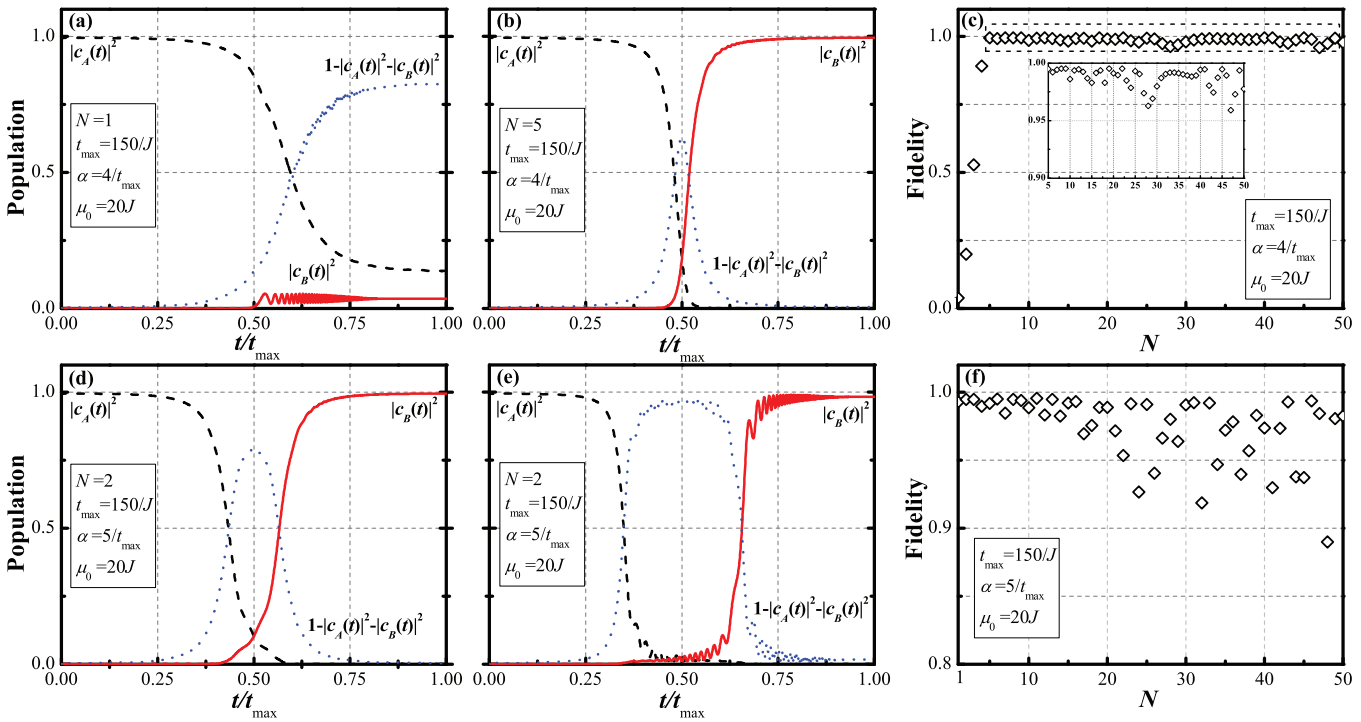


FIG. 6. (Color online) Time evolution of the initial state $|\Psi(0)\rangle = |A\rangle$. Population transfer as a function of time obtained for two different standard deviation of the control pulse: $\alpha = 4/t_{\max}$ (a)–(c) and $\alpha = 5/t_{\max}$ (d)–(f). Population transfer as a function of time obtained for two path number: (a) $N = 1$ and (b) $N = 5$. The dashed, black curve represents the probability of $|A\rangle$ on state $|\Psi(t)\rangle$. The red, solid curve represents the probability of state $|B\rangle$ on state $|\Psi(t)\rangle$. The population on other media dots is shown as blue, dotted curve. (c) Final population of state $|B\rangle$ plotted against the path number $N$. The small rectangular part is magnified in the inset. (d)–(f) are the same as in (a)–(c), but for $\alpha = 5/t_{\max}$ and $N = 2$ (d) and $N = 5$ (e). The transfer fidelity in part (d) is 99.5% and 99% in (e). (f) The transfer dynamics becomes unstable as the pathway number increases. The values of parameters chosen are shown in the figure.

### D. Discussion

We have proposed a scheme for transporting a single electron between two nonadjacent QDs through slowly manipulating the on-site energies. Initially, the electron is loaded into the left QD and driven by the external gate voltages to the aim dot. Strictly speaking, the multipath data bus we introduced here acts like a beam splitter. Our scheme may make some contributions to fundamental issues in physics like quantum control, the interference of single electron, and especially quantum state transfer.

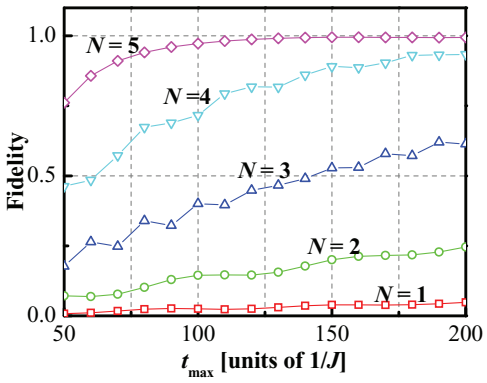


FIG. 7. (Color online) Fidelity as a function of $t_{\max}$ (in units of $1/J$) for (bottom to top along fidelity axis) 1-, 2-, 3-, 4-, 5-path systems with peak value $\mu_0 = 20J$.

We choose a Gaussian pulse to modulate the gate voltages. The parameters are $\mu_0 = 20J$, $t_{\max} = 150/J$, and $\alpha = 4/t_{\max}$, $5/t_{\max}$. For $\alpha = 4/t_{\max}$, one can see the transfer fidelity increases as the pathway number grows, as shown in Fig. 6(c). However, the fidelity for the case $N > 5$ nearly has not been improved compared with the case $N = 5$. Therefore, this case will not be considered further. The results show that it

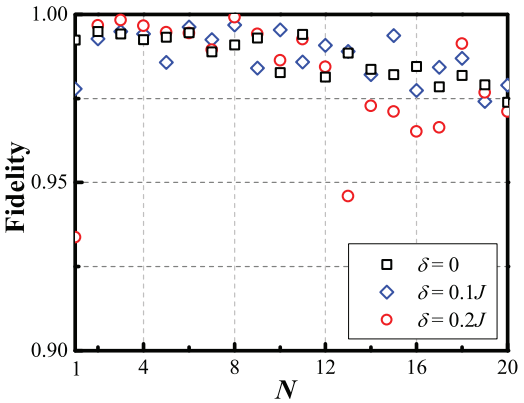


FIG. 8. (Color online) Plot of transfer fidelity as a function of pathway number by considering the fabrication errors for maximum coupling offset bias $\delta = 0$ (open square), $\delta = 0.1J$ (open diamond), and $\delta = 0.2J$ (open circle). The parameters we chosen are $\mu_0 = 20J$, $t_{\max} = 150/J$, and $\alpha = 4/t_{\max}$.

is possible to enhance the transfer efficiency by introducing a multipath data bus, which is one of the main results of this work. Compared with Fig. 6(c), Fig. 6(f) shows that the optimal value for the number of paths is different for different controlling protocols. Moreover, we also investigate our proposal in a more realistic QD system in the presence of inevitable fabrication imperfections. Based on the parameters previously discussed in Fig. 6(c), we add a random offset bias $\delta\epsilon_j$ to the couplings in each pathway. As an example, the effect of offset on adiabatic QST is shown in Fig. 8 for two cases: $\delta = 0.1J$ and $0.2J$. One can see that small offset is unimportant in this proposal.

## IV. CONCLUSION

Limited by the inevitable decoherence of the quantum system, a quantum computer should be able to perform a large number of high-fidelity quantum state transfers within the finite decoherence time. Therefore, much attention should be devoted to explore a high-efficiency data bus or proposal for adiabatic QST.

In such a scheme, all the system parameters are time independent except for two-end on-site energies. This makes it possible to investigate a variety of special geometry in Hilbert spaces. In this proposal we introduce a multipath data bus for adiabatic QST and discuss its transfer efficiency. First, we have shown that the evolution of the system is restricted on a five-dimensional Hilbert subspace by using linear transformation. Then we have numerically demonstrated that it is possible to enhance the quantum state transfer efficiency by setting up a multipath data bus. The optimal path number and corresponding shortest possible time for high-fidelity transfer are determined from the numerical way. Moreover, the robustness of the scheme to fabrication disorder is demonstrated.

## ACKNOWLEDGMENTS

One of the author (B.C.) thanks Professor Lan Zhou (Hunan Normal University) for helpful discussions. We acknowledge the supports of the NSF of China (Grants No. 11105086 and No. 11204162), the Shandong Provincial Natural Science Foundation (Grants No. BS2011DX029 and No. ZR2012FQ001), the basic scientific research project of Qingdao (Grant No. 11-2-4-4-(6)-jch), and SDUST Research Fund (2012KYTD103). We also acknowledge the support by Shandong Philosophy Planning Project (Grant No. 11CZXJ02).

[1] K. Bergmann, H. Theuer, and B. W. Shore, Rev. Mod. Phys. **70**, 1003 (1998).
[2] A. D. Greentree, J. H. Cole, A. R. Hamilton, and L. C. L. Hollenberg, Phys. Rev. B **70**, 235317 (2004).
[3] K. Eckert, M. Lewenstein, R. Corbalán, G. Birkl, W. Ertmer, and J. Mompart, Phys. Rev. A **70**, 023606 (2004).
[4] S. Longhi, G. Della Valle, M. Ornigotti, and P. Laporta, Phys. Rev. B **76**, 201101(R) (2007).
[5] F. Dreisow, A. Szameit, M. Heinrich, R. Keil, S. Nolte, A. Tünermann, and S. Longhi, Opt. Lett. **34**, 2405 (2009).
[6] N. V. Vitanov and B. W. Shore, Phys. Rev. A **73**, 053402 (2006).
[7] K. Eckert, J. Mompart, M. Lewenstein, R. Corbalán, and G. Birkl, Opt. Commun. **264**, 264 (2006).
[8] W. Merkel, H. Mack, M. Freyberger, V. V. Kozlov, W. P. Schleich, and Bruce W. Shore, Phys. Rev. A **75**, 033420 (2007).
[9] S. McEndoo, S. Croke, J. Brophy, and Th. Busch, Phys. Rev. A **81**, 043640 (2010).
[10] L. C. L. Hollenberg, A. D. Greentree, A. G. Fowler, and C. J. Wellard, Phys. Rev. B **74**, 045311 (2006).
[11] E. M. Graefe, H. J. Korsch, and D. Witthaut, Phys. Rev. A **73**, 013617 (2006).
[12] M. Rab, J. H. Cole, N. G. Parker, A. D. Greentree, L. C. L. Hollenberg, and A. M. Martin, Phys. Rev. A **77**, 061602(R) (2008).
[13] J. Siewert, T. Brandes, and G. Falci, Opt. Commun. **264**, 435 (2006).
[14] L. M. Jong, A. D. Greentree, V. I. Conrad, L. C. L. Hollenberg, and D. N. Jamieson, Nanotechnology **20**, 405402 (2009).
[15] I. Kamleitner, J. Cresser, and J. Twamley, Phys. Rev. A **77**, 032331 (2008).
[16] A. D. Greentree, S. J. Devitt, and L. C. L. Hollenberg, Phys. Rev. A **73**, 032319 (2006).
[17] L. M. Jong and A. D. Greentree, Phys. Rev. B **81**, 035311 (2010).
[18] J. H. Cole, A. D. Greentree, L. C. L. Hollenberg, and S. Das Sarma, Phys. Rev. B **77**, 235418 (2008).
[19] Tomáš Opatrný and Kunal K. Das, Phys. Rev. A **79**, 012113 (2009).
[20] P. Zhang, Q.-K. Xue, X.-G. Zhao, and X. C. Xie, Phys. Rev. A **69**, 042307 (2004).
[21] B. Chen, W. Fan, and Y. Xu, Phys. Rev. A **83**, 014301 (2011).
[22] B. Chen, W. Fan, Y. Xu, Z.-Y. Chen, X.-L. Feng, and C. H. Oh, Phys. Rev. A **86**, 012302 (2012).
[23] B. Chen, Q.-H. Shen, W. Fan, and Y. Xu, Sci. China-Phys. Mech. Astron. **55**, 1635 (2012).
[24] M. Christandl, N. Datta, A. Ekert, and A. J. Landahl, Phys. Rev. Lett. **92**, 187902 (2004).
[25] M. Christandl, N. Datta, T. C. Dorlas, A. Ekert, A. Kay, and A. J. Landahl, Phys. Rev. A **71**, 032312 (2005).